Original scientific paper

New modified mesoporous silica nanoparticles with bimetallic Ni-Zr for electroanalytical detection of dopamine

Mohamad Rafizie Aiman Mohamed Roduan[1], Mohamad Idris Saidin[1,✉], Siti Munirah Sidik[1], Jaafar Abdullah[2], Illyas Md Isa[1], Norhayati Hashim[1], Mohamad Syahrizal Ahmad[1], Siti Nur Akmar Mohd Yazid[1], Anwar Ul-Hamid[3] and Aireen Aina Bahari[4]

[1]Department of Chemistry, Faculty of Science and Mathematics, Universiti Pendidikan Sultan Idris, 35900 Tanjong Malim, Perak, Malaysia

[2]Department of Chemistry, Faculty of Science, Universiti Putra Malaysia, 43400 Seri Kembangan, Selangor, Malaysia

[3]Materials Characterization Laboratory, Centre for Engineering Research, Research Institute, King Fahd University of Petroleum and Minerals, Dhahran 31261, Saudi Arabia

[4]Department of English Language and Literature, Faculty of Languages and Communication, Universiti Pendidikan Sultan Idris, 35900 Tanjong Malim, Perak, Malaysia

Corresponding author: ✉*idris.saidin@fsmt.upsi.edu.my; Tel.: +6015 4879 7958*

Abstract

In this research, bimetallic nickel-zirconia supported on mesoporous nanoparticles (Ni-Zr/MSN) were successfully synthesized by a simple in situ electrolysis method. Ni-Zr/MSN were well-characterized by Fourier transform infrared spectroscopy (FTIR), X-ray diffraction (XRD), X-ray photoelectron spectroscopy (XPS), Brunauer-Emmett-Teller (BET) analyzer, field emission scanning electron microscopy (FESEM), and transmission electron microscopy (TEM). Ni-Zr/MSN were then cast onto a modified glassy carbon electrode (Ni-Zr/MSN/GCE) as dopamine (DA) sensor. Under optimal conditions, the sensor showed a linear concentration relationship in the range of 0.3 µM–0.1 mM with a limit of detection of 0.13 µM. The relative standard deviation for 0.1 mM DA solution was 2.1 % (n = 5). The presence of excess catechol, saccharose, glycine, lactose, uric acid, and Cr^{3+}, Fe^{2+} and Na^+ as interferents was negligible, except for uric acid in 10-fold excess. The analytical recovery of the sensor was successfully demonstrated by the determination of DA in DA-containing medicine and wastewater samples. The results presented herein provide new perspectives on Ni-Zr/MSN as a potential nanomaterial in the development of DA sensors.

Introduction

Dopamine (DA), which is an important chemical found in human bodies, helps cells to transmit impulses to the receptor other than functioning as a catecholamine neurotransmitter [1]. DA helps in regulating the central nervous system and the cardiovascular system, where an abnormal DA level can cause vital problems in the mammalian body [2–4]. Abnormal DA level often contributes to schizophrenia, Parkinson's disease, attention deficit hyperactivity disorder, euphoria, and Alzheimer's and Huntington's diseases [1–7]. Individuals suffering from mental illness are more prone to coronavirus (COVID-19) when they have difficulties comprehending protective measures such as frequent handwashing, social distancing, and isolation than normal persons [8]. Research conducted on 50,750 COVID-19 patients in France by Mohan *et al.* [9], found that 1.6 % had schizophrenia. The data revealed an alarming increase in the lifetime prevalence of schizophrenia in the West [9]. Hence, a rapid, accurate and simple method to detect DA levels is demanded. Formerly, chromatography [10], fluorometry [11], chemiluminescence analysis [12], colorimetry [13], and electrochemistry [14-16] were employed to detect DA. However, various researchers proved that only electrochemical techniques have simple operation and fast response, being at the same time eco-friendly, cost-effective, mobile, highly sensitive and highly selective [17,18].

In electrochemical analysis, the electrode material acts as the main factor influencing the performance of the sensor. Due to the special traits that certain sensors have, the traits will help enhance the electrochemical analysis for the detection of the desired element [19]. Various types of electrochemical sensors have been developed to detect DA, such as reduced graphene oxide (RGO) [20], gold nanoparticles/polyaniline-modified GSPEs (AuNPs@PANI/GSPEs) [21], calcium stannate-graphitic carbon nitride nanohybrid material (CSO-gCN) [22], poly(3,4-ethylenedioxythiophene) modified laser scribed graphene (PEDOT-LSG) [23], single-walled carbon nanotubes array-modified glassy carbon electrode (SWCNTs array-GCE) [24], reduced graphene oxide with manganic manganous oxide (rGO-Mn_3O_4) [25] and polymerization-modified carbon paste electrodes [26-29]. However, these sensors have several drawbacks, such as narrow working concentration ranges and low sensitivity and selectivity. Mesoporous silica nanoparticles (MSN) are one of the essential elements in sensor modification, as MSN has a large surface area easily doped with metals, equally sized pores and ordered structure [30].

Although various attempts have been made in the development of electrochemical sensors using MSN, there is a lack of studies on the use of MSN modified by a bimetal as an electrochemical sensor for DA detection. Therefore, in this research, a newly synthesized nickel-zirconia doped with mesoporous silica nanoparticles (Ni-Zr/MSN) was successfully fabricated as a modified GCE sensor for DA detection. The performance of the sensor could provide a new perspective on the modified MSN as a potential nanomaterial in the field of electrochemical sensors.

Experimental

Materials and reagents

All chemicals used in the synthesis of Ni-Zr/MSN and electrochemical sensing experiments were of analytical grade (Merck and Sigma-Aldrich) and used without further purification. Ethanol, methanol, *N,N*-dimethylformamide, cetyltrimethylammonium bromide, ethylene glycol, ammonium hydroxide, tetraethyl orthosilicate, 3-aminopropyl triethoxysilane and disodium phosphate (Na_2HPO_4) were purchased from Merck. Monosodium phosphate (NaH_2PO_4), catechol, glycine, uric acid, lactose, saccharose, chromium (III) chloride ($CrCl_3$), iron (II) sulfate ($FeSO_4$), sodium chloride

(NaCl), and dopamine hydrochloride were purchased from Sigma-Aldrich. The distilled deionized water from EASYpure LF, Barnstead, was used to wash synthesized Ni-Zr/MSN and prepare all analytical solutions. The supporting electrolyte was 0.1 M phosphate buffer solution (PBS) prepared by mixing stock solutions of Na_2HPO_4 and NaH_2PO_4.

Apparatus

Cyclic voltammetry and differential pulse voltammetry were performed using a Potentiostat Interface 1010B (Gamry, USA). Three-electrode system consisting of Ag/AgCl (3M KCl) reference electrode MF-2052 with (Bioanalytical System, USA), counter electrode of platinum wire, and Ni-Zr/MSN GCE as the working electrode was used in all electrochemical measurements. The pH of a solution was determined using an Orion 720A glass electrode (Mass., USA). The characteristics of Ni-Zr/MSN were studied using a Fourier transform infrared (FTIR) spectrophotometer model Cary 630 (Agilent, USA), an X-ray diffraction (XRD) instrument model Rigaku 600 (MiniFlex, Japan), an X-ray photoelectron spectroscopy (XPS) instrument model PHI Quantera II (ULVAC-PHI, Japan), energy-dispersive X-ray spectroscopy (EDX) model SU 8030 UHR (Hitachi, Japan) and a Brunauer-Emmett-Teller (BET) analyzer model Tristar II Plus (Micromeritics, USA). The XRD data were analyzed using Rigaku SmartLab Studio II software. Electrochemical impedance spectroscopy (EIS) measurements were carried out using a potentiostat/galvanostat model Ref 3000 (Gamry, USA). EIS measurements were performed in the frequency range of 1.0 MHz to 1.0 Hz with 5.0 mV of alternating signal amplitude. Finally, the surface morphology of Ni-Zr/MSN was characterized by a Field-emission scanning electron microscope (FESEM) model SU8030 (Hitachi, Japan) and a transmission electron microscope (TEM) model JEM 2100F (JOEL, Japan).

Synthesis of Ni-Zr/MSN

Co-condensation and sol-gel methods were implemented to synthesize MSN. A mixture of cetyltrimethylammonium bromide, ethylene glycol, and ammonium hydroxide solutions was vigorously stirred for 30 min at 50 °C. Then, 1.2 mmol tetraethyl orthosilicate and 1 mmol 3-aminopropyl triethoxysilane were added to the homogenous mixture. This solution was stirred for another 2 h at 80 °C and dried at 110 °C overnight. A white powder of MSN was collected after being dried and calcined at 550 °C for 3 h to remove impurities.

Preparation of Ni-Zr/MSN was done by in situ electrolysis method where the platinum (Pt, Nilaco) and zirconia/nickel plates were used as the anode and the cathode, respectively. 30 mL of *N,N*-dimethylformamide (DMF) solution was added to tetraethylammonium perchloride (TEAP), naphthalene, and 1.5 g of MSN. Electrolysis was then performed under continuous stirring at the constant current density of 480 mA cm^{-2} and 0 °C under a nitrogen atmosphere. The Ni-Zr/MSN collected at the cathode was heated at 85 °C before drying overnight at 110 °C. Finally, the sample was calcined at 550 °C for 3 h.

Preparation of Ni-Zr/MSN/GCE modified electrode

The surface of GCE was first polished using an alumina slurry (0.05 μm) sequentially, washed ultrasonically in ethanol and deionized water before modification with Ni-Zr/MSN. The Ni-Zr/MSN (2.5, 5.0, and 7.0 mg) was mixed in 10 mL DMF solution and ultrasonicated for 30 min and 2.5 μL of the suspension was drop-casted on the GCE surface. The electrode was allowed to dry at room temperature. As a result, Ni-Zr/MSN modified GCE known as Ni-Zr/MSN/GCE was obtained. Similar procedures were applied for the preparation of unmodified GCE (bare GCE) but without the addition of Ni-Zr/MSN.

Results and discussion

Characterization of Ni-Zr/MSN

Figure 1(a) shows the FTIR spectrum of Ni-Zr/MSN recorded in the range of 4000 to 400 cm^{-1}. The absorption band at ~1056 cm^{-1} was assigned to the asymmetric and symmetric stretching vibrations of Si-O-Si. The addition of bimetallic elements (*e.g.*, Ni and Zr) has possibly formed interaction with Si-O-Si group due to desilication [31]. As shown in Figure 1(b), four diffraction peaks representing NiO were observed at 37.3 (003), 43.3 (012), 62.9 (104), and 75.4° (015). A small diffraction peak was also observed at 79.4° (440), attributing to the characteristic peak of Ni$_4$ZrO phase and possibly indicating that existence of this phase facilitates the formation of Ni-Zr alloy.
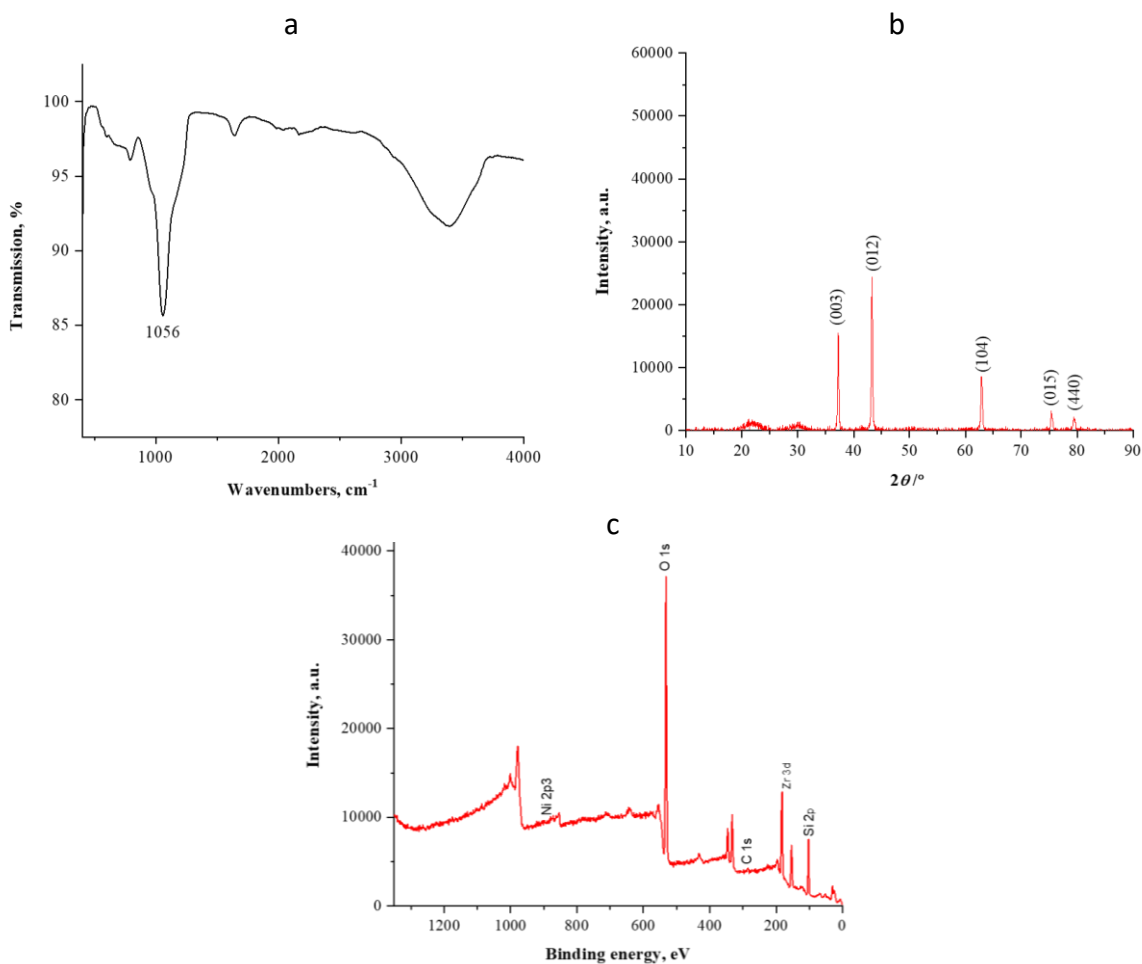

Figure 1. *(a) FTIR spectrum, (b) XRD patterns and (c) XPS spectrum of Ni-Zr/MSN*

Next, XPS wide scan analysis, as shown in Figure 1(c), the sample surface consists of Ni, Zr, C, Si, and O with binding energies of Ni2p3, Zr3d, C1s, Si2p, and O1s at 854, 182, 285, 103, and 532 eV, respectively. In the Ni2p3 region, the spectra were fitted with a single deconvoluted peak at 855 eV, which could be assigned to metallic Ni(OH)$_2$ (Ni^{2+}) species. The Zr3d spectra exhibited peaks at 182 and 183 eV for the presence of Zr metallic ZrO$_2$ (Zr^{2+}) and ZrOH (Zr$^+$) deconvolution, respectively. For the Si2p spectra, only a single deconvolution occurred (*i.e.,* SiO$_2$ (Si^{2+})), which exhibited a peak at 103 eV. Thus, the results confirm that Ni and Zr have been successfully loaded into the MSN. This result implies a d-electron transfer between Ni and Zr in the Ni-Zr/MSN, resulting in the enrichment of electrons on elemental Ni [32].

Figure 2 shows the morphology of Ni-Zr/MSN as characterized by scanning electron microscopy (SEM). Uniformed size distribution of Ni-Zr/MSN could be observed in the range of 25.9–68.8 nm.

Additionally, the SEM image also reveals new trigonal bipyramidal particles corresponding to a possible interaction between Ni and Zr, which was later confirmed by EDX mapping analysis (Figure 3). The analysis confirmed that Ni and Zr are the main components in this trigonal bipyramidal structure.
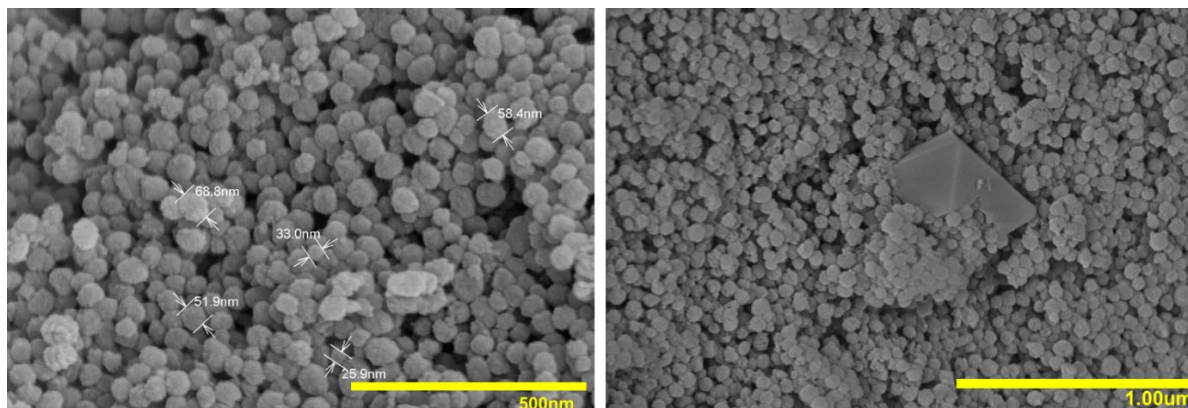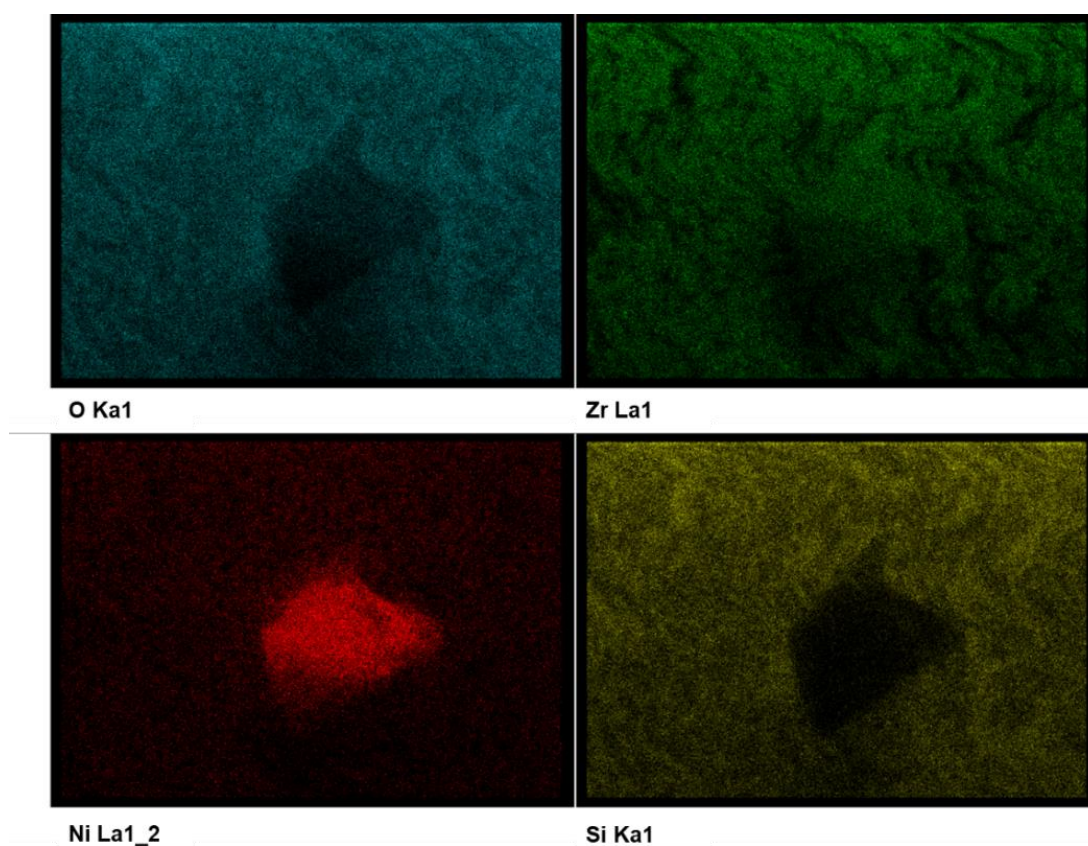

Figure 2. *SEM images of Ni-Zr/MSN*

Figure 3. *EDX-mapping of Ni-Zr/MSN*

The TEM image (Figure 4) shows that Ni and Zr were doped in the ordered porous framework of spherical MSN, protecting themselves from aggregation. Then, the selected area electron diffraction (SAED) (Figure 4, inset) spot pattern shows two characteristic diffraction rings, indicating the crystalline nature of Ni-Zr/MSN. The porosity of Ni-Zr/MSN was identified through the BET surface area analysis. Prior to the analysis, Ni-Zr/MSN was degassed at 300 °C for 1 h to obtain more accurate results on the pore size and BET surface area. From the analysis, the Langmuir surface area was 594.43 $m^2\,g^{-1}$ and the micropore volume was 0.03559 $cm^3\,g^{-1}$, which indicates a good pore size of Ni-Zr/MSN, which allows bimetallic elements to be doped into it as previously reported [33].
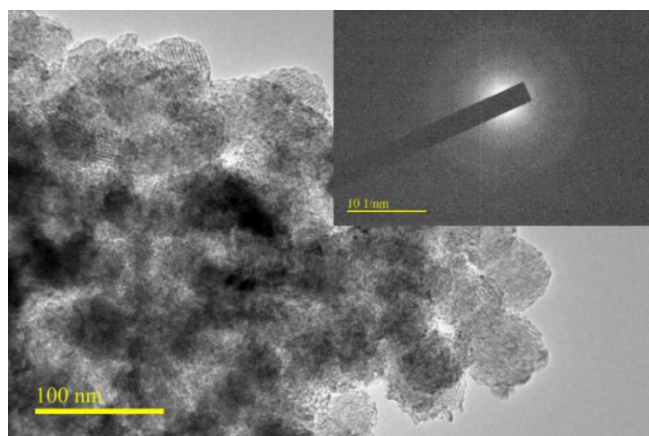
Figure 4. *TEM image and SAED pattern (inset) of Ni-Zr/MSN*

Electrochemical behavior of Ni-Zr/MSN/GCE

The electrochemical behavior of Ni-Zr/MSN/GCE was evaluated by CV and EIS analyses. The CV voltammogram of Ni-Zr/MSN/GCE in the absence and presence of 0.1mM DA in 0.1 M PBS (pH 7.0) is shown in Figure 5. As seen, no redox peak current is observed in the absence of DA (curve a), but a significant redox peak current is observed in the presence of DA (curve b). This means that the sensor shows a sensitive response in the presence of DA. The comparison of CV response between Ni-Zr/MSN/GCE and bare GCE in 0.1 mM DA and 0.1 M PBS (pH 7.0) as a supporting electrolyte was also evaluated. As illustrated in Figure 5, the CV peak current at Ni-Zr/MSN/GCE (curve b) indicated higher current reading than bare GCE (curve c) due to the increase of electron transfer rate and conductivity on the electrode surface. The anodic peak current (I_{pa}) and cathodic peak current (I_{pc}) of bare GCE were 2.649 and 2.637 μA, respectively. Meanwhile, the redox peak current of Ni-Zr/MSN/GCE increased to 5.789 μA for I_{pa} and 6.166 μA for I_{pc}. The peak-to-peak separation (ΔE_p) of Ni-Zr/MSN/GCE also decreases to 60.00 mV compared to bare GCE, which has ΔE_p of 240.01 mV. Therefore, the results showed that Ni-Zr/MSN/GCE has good electrocatalytic activity and good selectivity, hence improving the electron transfer rate and electrochemical response [34].
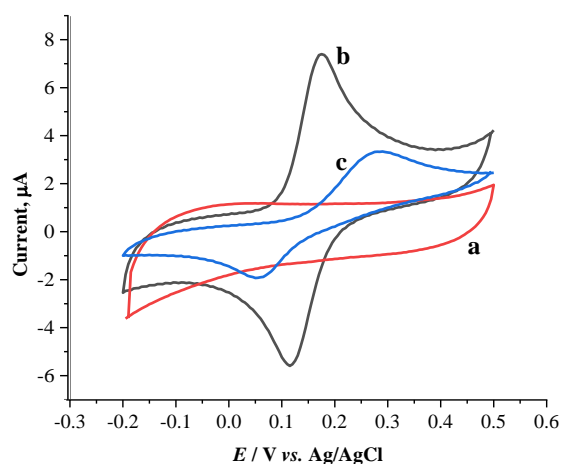

Figure 5. *CV voltammograms of Ni-Zr/MSN/GCE in the absence (curve a) and in presence (curve b) of 0.1 mM DA in 0.1 M PBS (pH 7.0). Curve c is CV voltammogram of bare GCE. Scan rate is 100 mV s⁻¹*

CV analysis was also conducted to study the reaction kinetics of Ni-Zr/MSN/GCE. The curves of CV responses towards DA at different scan rates are plotted in Figure 6a. Plots of anodic and cathodic peak currents versus the scan rate as illustrated in Figure 6b, showing straight lines with linear equations defined as follows: I_{pa} (μA) = 0.0297 v (mV s⁻¹) + 6.2519 (R^2 = 0.9685) and I_{pc} (μA) =

-0.031 v (mV s^{-1}) – 5.2176 (R^2 = 0.9396). It could be observed that the increasing scan rate from 90 to 400 mV s^{-1} resulted in the gradual potential shift of the oxidation peak toward positive values. These results suggest that the oxidation reaction of DA at Ni-Zr/MSN/GCE is predominantly an adsorption-controlled process.
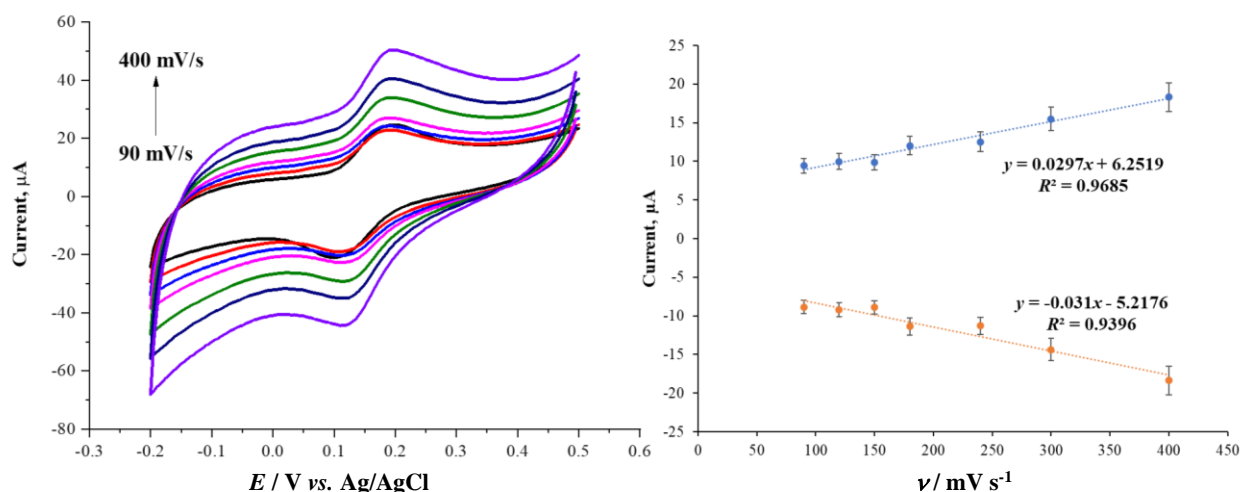

Figure 6. *CV voltammograms of 0.1 mM DA in 0.1 M PBS (pH 7.0) on Ni-Zr/MSN/GCE at (a) various scan rates (90-400 mV/s) and (b) corresponding plots of anodic and cathodic peak currents vs. scan rate*

The performance of Ni-Zr/MSN/GCE at different amounts of Ni-Zr/MSN was also evaluated in order to determine the optimized amount of Ni-Zr/MSN drop-casted on the GCE surface. Figure 7(a) shows that 0.625 µg of Ni-Zr/MSN achieved a higher current response; hence, Ni-Zr/MSN increased the charge transfer kinetics, thus enhancing the performance of Ni-Zr/MSN/GCE. Nevertheless, further addition of Ni-Zr/MSN (1.25 and 1.75 µg) reduced the current response, which might be the result of oversaturated modifier loading at the electrode surface. Thus, 0.625 µg of Ni-Zr/MSN was utilized as a modifier in the subsequent analysis.

The interfacial properties of bare GCE and Ni-Zr/MSN/GCE were evaluated through the EIS-Nyquist plots shown in Figure 7(b).
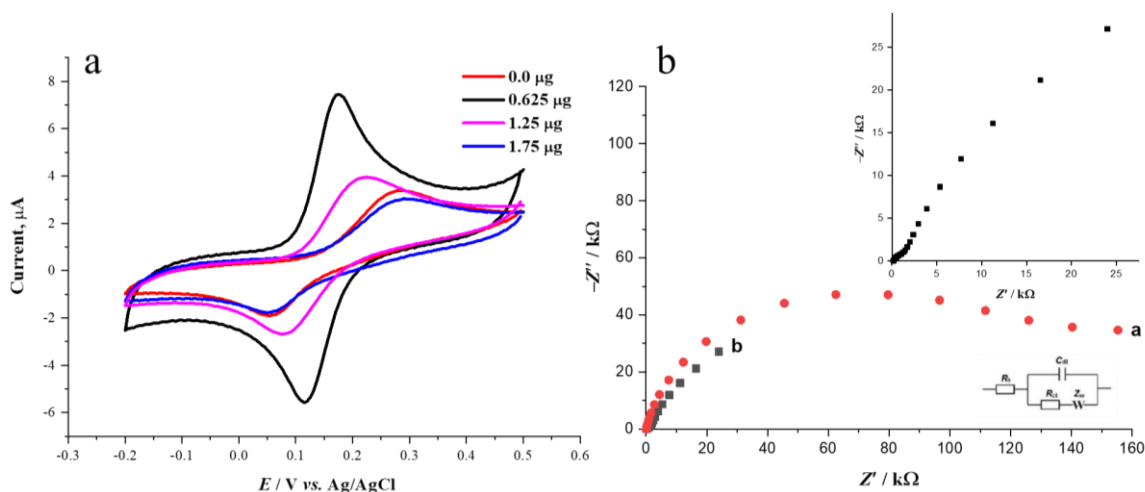

Figure 7. *(a) CV voltammograms of 0.1 mM DA in 0.1 M PBS (pH 7.0) on Ni-Zr/MSN/GCE at different quantities of Ni-Zr/MSN; (b) Nyquist plots of bare GCE (curve a) and Ni-Zr/MSN/GCE (0.625 µg) (curve b). Inset (top-right): enlarged Nyquist plot of Ni-Zr/MSN/GCE. Frequency range: 1.0 MHz to 1.0 Hz. Inset (bottom-right): Randles equivalent circuit model used to fit impedance data*

Generally, a diameter of semicircle impedance response at higher frequencies represents the charge transfer resistance, while a linear part at lower frequencies represents the diffusion process [35]. As illustrated in Figure 7b, the Nyquist plot of the bare GCE exhibits a larger semicircle (curve a) compared to Ni-Zr/MSN/GCE (curve b), indicating lower charge transfer resistance in the interfacial region of Ni-Zr/MSN/GCE. By fitting the Randles equivalent electrical circuit (Figure 7b, inset), charge transfer resistance (R_{ct}) values for bare GCE and Ni-Zr/MSN/GCE were 106.4 and 0.613 kΩ. Additionally, the electron transfer apparent rate constant (k_{app}) values [36] calculated for bare GCE and Ni-Zr/MSN/GCE were 2.50×10^{-8} and 4.34×10^{-6} cm s^{-1}. The high k_{app} and low R_{ct} values for Ni-Zr/MSN/GCE indicate a fast electron transfer process facilitated by Ni-Zr/MSN [37]. The EIS results correlate with the finding of CV studies.

Effect of pH

The performance of Ni-Zr/MSN/GCE in 0.1 mM DA in 0.1 M PBS at different pH values was investigated in the range of pH 6.0–8.0 using the differential pulse voltammetry (DPV) method. The graph of I_{pa} versus pH is shown in Figure 8. The oxidation current for DA reached the most optimized state at pH 7.0, which is a neutral buffer state. There was a slight improvement from pH 7.6 to 8.0, but it was still inferior to the current reading for pH 7.0. The decreased peak current beyond pH 7.0 could be attributed to the deprotonation of DA, and at pH below 7.0, the decrease could be due to protonation [38]. Thus, the PBS pH of 7.0 was chosen as an optimized pH for further measurements of the study.
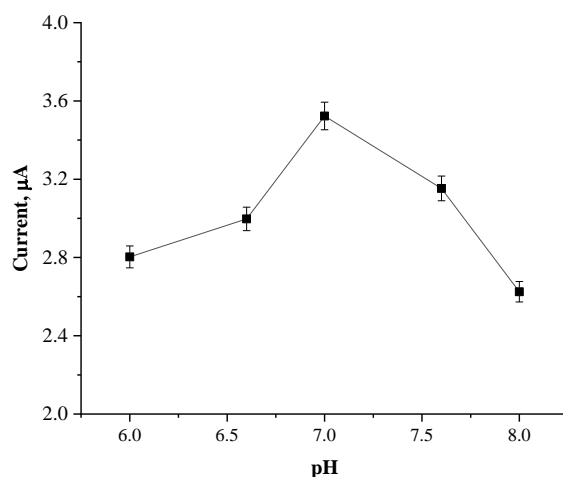

Figure 8. *Effects of various pH on DPV peak current of 0.1 mM DA in 0.1 M PBS at Ni-Zr/MSN/GCE. Frequency: 100 Hz; step increment: 3.0 mV; pulse size: 120 mV*

Electrochemical performance for dopamine detection

Under optimal analysis conditions, the analytical curve of DA was constructed from the DPV quantification carried out at different DA concentrations. From Figure 9(a), the peak voltammogram for DA increased with the increase of DA concentration in the range from 0.3 μM to 0.1 mM. The linear regression equation I_{pa} (μA) = 28.073 DA + 0.0506 with R^2 of 0.9929 was obtained within this concentration range (Figure 9(b)). The limit of detection of 0.13 μM was estimated using the formula of $3 S_b/m$, where S_b is the standard deviation obtained from five measurements of the blank signal and m is the slope of the linear calibration curve. It seems that the results obtained in this work are more worthy than those reported earlier (Table 1). The reproducibility of Ni-Zr/MSN/GCE was evaluated by five replicate measurements of 0.1 mM DA, and Ni-Zr/MSN/GCE showed good reproducibility where the relative standard deviation of 2.1 % (n = 5) was obtained.
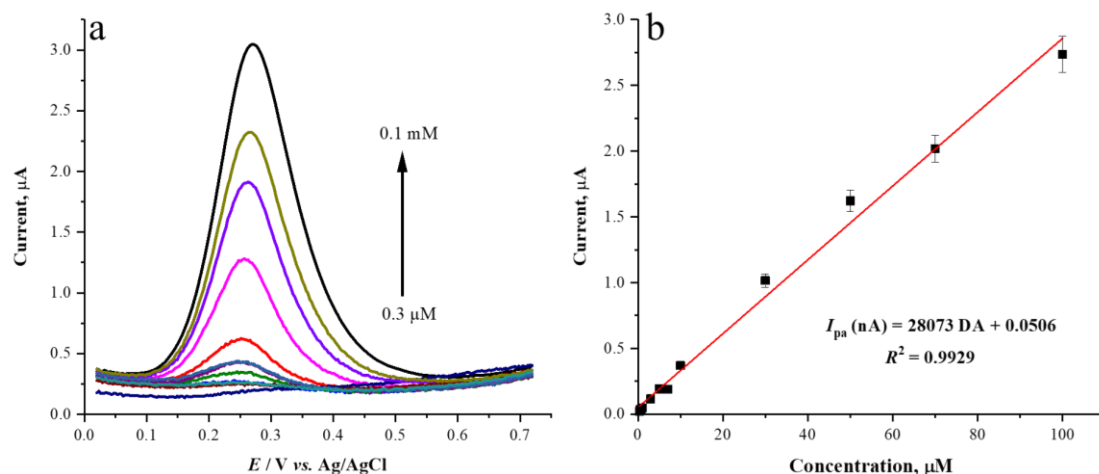
Figure 9. (a) DPV voltammograms and (b) corresponding calibration plot of 0.3 µM - 0.1 mM DA in 0.1 M PBS (pH 7) at Ni-Zr/MSN/GCE

Table 1. Comparison of Ni-Zr/MSN/GCE with other reported DA sensors

Electrode	Technique	LOD, µM	Linear range, µM	Ref.
RGO-CB-CTS/GCE	SWV	0.20	3.2 - 32	[20]
AuNPs@PANI/GSPEs	DPV	0.86	1 - 100	[21]
CSO-gCN/GCE	DPV	29	100 - 800	[22]
PEDOT-LSG	DPV	0.33	1 - 150	[23]
SWCNTs array-GCE	SWV	0.82	10 - 200	[24]
GE/rGO-Mn$_3$O$_4$/Nafion-Au	Amperometric	0.25	1 - 1450	[25]
Poly (adenine) film-CPE	CV	0.67	20 - 190	[28]
Ni-Zr/MSN/GCE	DPV	0.13	0.3 - 100	This work

Interference study

The possible interference for DA detection was investigated by adding some organic compounds and inorganic ions that may coexist with DA in real samples. The potential interferents used were catechol, saccharose, glycine, lactose, uric acid, and Cr^{3+}, Fe^{2+}, and Na^+ ions. Under optimal conditions, DPV measurements were performed for DA concentration established at 0.1 mM, while concentrations of interferents were kept at 0.1 and 1.0 mM in 0.1 M PBS (pH 7). As shown in Table 2, Ni-Zr/MSN/GCE demonstrated good anti-interference behavior, except for 10-fold excess of uric acid (the criterion for interference was a ±20 % error in the peak height of DA).

Table 2. Interference of potential interferents at concentrations of 0.1 mM and 1.0 mM (pH 7)

Interferers	Interference, %	
	DA content = 0.1 mM	PBS content = 1.0 mM
Catechol	5.98	12.59
Saccharose	8.68	12.4
Glycine	1.82	7.28
Lactose	2.75	3.83
Uric acid	10.02	25.6
Na$^+$	1.1	4.3
Fe^{2+}	2.31	10.63
Cr^{3+}	2.01	12.19

Recovery analysis

In an attempt to test the applicability of Ni-Zr/MSN/GCE, a recovery study of the DA-controlled medicine and wastewater samples were performed by the standard addition method. 1 mL of 0.01

mM DA-containing medicine was diluted with 0.1 M PBS and a known amount of DA solution was added after the original concentration of DA in the prepared sample was detected. Next, wastewater samples from two different locations were collected and the residue was filtered. 10 mL of filtered wastewater samples were diluted with 0.1 M PBS and a known amount of DA solution was added. Table 3 shows satisfactory recovery percentages in the range between 96.0 and 107.6 %, indicating that Ni-Zr/MSN/GCE is capable for the quantification of DA in real samples.

Table 3. Detection of DA in DA-containing medicine and wastewater samples (n= 3) using Ni-Zr/MSN/GCE

Sample	DA content, µM			Recovery, %
	Original	Added	Found	
DA-containing medicine	10	10	20.0 ± 0.5	100.0
	10	30	40.3 ± 0.2	103.1
Wastewater 1	0	10	9.6 ± 0.2	96.0
	0	30	29.1 ± 0.3	97.0
Wastewater 2	0	10	10.3 ± 0.2	103.0
	0	30	32.3 ± 0.5	107.6

Conclusions

The modified mesoporous silica nanoparticles (MSN) with bimetallic nickel-zirconia have been successfully synthesized using electrodeposition technique. Characterization by FT-IR, XRD, XPS, BET, TEM and FESEM surface techniques confirmed the formation of a highly porous system with a uniform particle size distribution of 25.9 and 68.8 nm, and the presence of Ni, Zr, Si and O in the prepared Ni-Zr/MSN nanomaterial. Different amounts of Ni-Zr/MSN were deposited on GCE and the prepared Ni-Zr/MSN/GCE was employed as an electrochemical sensor for DA determination. The CV and EIS studies of the sensor showed an excellent response and increased charge transfer rate of DA oxidation at the electrode-solution interface. The sensor displayed an excellent response in the working DA concentration range of 0.3 µM–0.1 mM, with a limit of detection of 0.13 µM with good reproducibility. The sensor also demonstrated good recovery for the analysis of DA in DA containing medicine and wastewater samples. This current work will help the scientific community to understand and realize a new perspective of modified MSN in the field of electroanalytical chemistry.

References

[1]   S. Yang, J. Zhao, S. Tricard, L. Yu, J. Fang, *Analytica Chimica Acta* **1094** (2020) 80-89. https://doi.org/10.1016/j.aca.2019.09.077

[2]   R. Sakthivel, S. Kubendhiran, S. M. Chen, J. V. Kumar, *Analytica Chimica Acta* **1071** (2019) 98-108. https://doi.org/10.1016/j.aca.2019.04.058

[3]   L. Jothi, S. Neogi, S. k. Jaganathan, G. Nageswaran, *Biosensors and Bioelectronics* **105** (2018) 236-242. https://doi.org/10.1016/j.bios.2018.01.040

[4]   J. Yang, Y. Hu, Y. Li, *Biosensors and Bioelectronics* **135** (2019) 224-230. https://doi.org/10.1016/j.bios.2019.03.054

[5]   Y. Li, J. Liu, M. Liu, F. Yu, L. Zhang, H. Tang, B. C. Ye, L. Lai, *Electrochemistry Communications* **64** (2016) 42-45. https://doi.org/10.1016/j.elecom.2016.01.009

[6]   S. Qi, B. Zhao, H. Tang, X. Jiang, *Electrochimica Acta* **161** (2015) 395-402. https://doi.org/10.1016/j.electacta.2015.02.116

[7] E. Nagles, J. A. Calderón, O. García-Beltrán, *Electroanalysis* **29(4)** (2017) 1081-1087. https://doi.org/10.1002/elan.201600729

[8] N. Kozloff, B. H. Mulsant, V. Stergiopoulos, A. N. Voineskos, *Schizophrenia Bulletin* **46** (2020) 752-757. https://doi.org/10.1093/schbul/sbaa051

[9] M. Mohan, B. I. Perry, P. Saravanan, S. P. Singh, *Frontiers in Psychiatry* **12** (2021) 666067. https://doi.org/10.3389/fpsyt.2021.666067

[10] D. Sangamithirai, S. Munusamy, V. Narayanan, A. Stephen, *Surfaces and Interfaces* **4** (2016) 27-34. https://doi.org/10.1016/j.surfin.2016.09.003

[11] A. Üğe, D. Koyuncu Zeybek, B. Zeybek, *Journal of Electroanalytical Chemistry* **813** (2018) 134-142. https://doi.org/10.1016/j.jelechem.2018.02.028

[12] Y. Li, H. Song, L. Zhang, P. Zuo, B. C. Ye, J. Yao, W. Chen, *Biosensors and Bioelectronics* **78** (2016) 308-314. https://doi.org/10.1016/j.bios.2015.11.063

[13] S. Wang, P. Guo, G. Ma, J. Wei, Z. Wang, L. Cui, L. Sun, A. Wang, *Electrochimica Acta* **360** (2020) 137016. https://doi.org/10.1016/j.electacta.2020.137016

[14] M. Cheng, X. Zhang, M. Wang, H. Huang, J. Ma, *Journal of Electroanalytical Chemistry* **786** (2017) 1-7. https://doi.org/10.1016/j.jelechem.2017.01.012

[15] P. Sankaranarayanan, S. V. Venkateswaran, *Journal of Electrochemical Science and Engineering* **10(3)** (2020) 263-279. https://doi.org/10.5599/jese.783

[16] H. Beitollahi, S. Tajik, M. R. Aflatoonian, A. Makarem, *Journal of Electrochemical Science and Engineering* **12(1)** (2022) 199-208. https://doi.org/10.5599/jese.1231

[17] X. Liu, E. Shangguan, J. Li, S. Ning, L. Guo, Q. Li, *Materials Science and Engineering: C* **70** (Part 1) (2017) 628–636. https://doi.org/10.1016/j.msec.2016.09.034

[18] D. Wang, F. Xu, J. Hu, M. Lin, *Materials Science and Engineering: C* **71** (2017) 1086-1089. https://doi.org/10.1016/j.msec.2016.11.023

[19] Z. Liu, M. Jin, J. Cao, R. Niu, P. Li, G. Zhou, Y. Yu, A. van den Berg, L. Shui, *Sensors and Actuators B: Chemical* **273** (2018) 873-883. https://doi.org/10.1016/j.snb.2018.06.123

[20] M. Baccarin, F. A. Santos, F. C. Vicentini, V. Zucolotto, B. C. Janegitz, O. Fatibello-Filho, *Journal of Electroanalytical Chemistry* **799** (2017) 436-443. https://doi.org/10.1016/j.jelechem.2017.06.052

[21] G. Selvolini, C. Lazzarini, G. Marrazza, *Sensors* **19(14)** (2019) 3097. https://doi.org/10.3390/s19143097

[22] S. Vinoth, R. Ramaraj, A. Pandikumar, *Materials Chemistry and Physics* **245** (2020) 122743. https://doi.org/10.1016/j.matchemphys.2020.122743

[23] G. Xu, Z. A. Jarjes, V. Desprez, P. A. Kilmartin, J. Travas-Sejdic, *Biosensors and Bioelectronics* **107** (2018) 184-191. https://doi.org/10.1016/j.bios.2018.02.031

[24] Y. Yang, M. Li, Z. Zhu, *Talanta* **201** (2019) 295-300. https://doi.org/10.1016/j.talanta.2019.03.096

[25] Z. Yao, X. Yang, Y. Niu, F. Wu, Y. Hu, Y. Yang, *Microchimica Acta* **184** (2017) 2081-2088. https://doi.org/10.1007/s00604-017-2210-7

[26] C. Raril, J. G. Manjunatha, *Current Topics in Electrochemistry* **21** (2019) 93-105.

[27] N. Hareesha, J. G. Manjunatha, *Journal of Electroanalytical Chemistry* **878** (2020) 114533. https://doi.org/10.1016/j.jelechem.2020.114533

[28] N.S. Prinith, J. G. Manjunatha, C. Raril, *Analytical and Bioanalytical Electrochemistry* **11(6)** (2019) 742-756. https://www.sid.ir/en/journal/ViewPaper.aspx?id=808521

[29] J. G. Manjunathaa, M. Deraman, N.H. Basri, I. A. Talib, *Advanced Materials Research* **895** (2014) 447-451. https://doi.org/10.4028/www.scientific.net/AMR.895.447

[30] Y. Xu, F. Y. H. Kutsanedzie, M. Hassan, J. Zhu, W. Ahmad, H. Li, Q. Chen, *Food Chemistry* **315** (2020) 126300. https://doi.org/10.1016/j.foodchem.2020.126300

[31] C. N. C. Hitam, A. A. Jalil, S. M. Izan, M. S. Azami, M.H. Hassim, N. Chanlek, *Powder Technology* **375** (2020) 397-408. https://doi.org/10.1016/j.powtec.2020.07.114

[32] K. Q. Jing, Y. Q. Fu, Z. N. Chen, T. Zhang, J. Sun, Z. N. Xu, G. C. Guo, *ACS Applied Materials & Interfaces* **12(21)** (2021) 24856-24864. https://doi.org/10.1021/acsami.1c04523

[33] R. Fiorenza, L. Spitaleri, A. Gulino, S. Scirè, *Catalysts* **8(5)** (2018) 203. https://doi.org/10.3390/catal8050203

[34] N. B. Messaoud, M. E. Ghica, C. Dridi, M. B. Ali, C. M. A. Brett, *Sensors and Actuators B: Chemical* **253** (2017) 513-522. https://doi.org/10.1016/j.snb.2017.06.160

[35] H. Jin, C. Zhao, R. Gui, X. Gao, Z. Wang, *Analytica Chimica Acta* **1025** (2018) 154–162. https://doi.org/10.1016/j.aca.2018.03.036

[36] I. D. Raistrick, D. R. Franceschetti, J. R. Macdonald, in: *Impedance Spectroscopy: Theory, Experiment and Applications, Second Edition*, J.R. Macdonald, E. Barsoukov (Eds.), Chap. 2, Wiley, 2005, pp. 27-128. https://doi.org/10.1002/0471716243.ch2

[37] N. A. Azis, I. M. Isa, N. Hashim, M. S. Ahmad, S. N. A. Mohd Yazid, M. I. Saidin, S. M. Si, R. Zainul, A. Ulianas, S. Mukdasai, *International Journal of Electrochemical Science* **14** (2019) 10607-10621. https://doi.org/10.20964/2019.11.46

[38] R. Moscoso, J. Carbajo, J. D. Mozo, J. A. Squella, *Journal of Electroanalytical Chemistry* **765** (2016) 149-154. https://doi.org/10.1016/j.jelechem.2015.08.010